JOURNAL OF GUIDANCE, CONTROL, AND DYNAMICS
Vol. 29, No. 5, September–October 2006

Peak-Seeking Control for Drag Reduction in Formation Flight

David F. Chichka*
George Washington University, Washington, D.C. 20052
Jason L. Speyer†
University of California, Los Angeles, Los Angeles, California 90095
Claudio Fanti‡
Università di Padova, 2-35122 Padova, Italy
and
Chan Gook Park§
Kwangwoon University, Seoul, 139-701, Republic of Korea

Formation flight is a known method of improving the overall aerodynamic efficiency of a pair of aircraft. In particular, one craft flying in the correct position in the vortex wake of another can realize substantial reductions in drag, with the amount of the reduction dependent on the relative positions of the two craft. This paper looks at such a pair, with one craft flying behind and to the side of the lead plane. The precise position of the second craft relative to the first to maximize the drag reduction is to be determined online, leading to a peak-seeking control problem. A new method of speak-seeking control, using a Kalman filter to estimate the characteristics of the drag reduction, is derived and discussed. A simple model of the two-plane formation using horseshoe vortices is defined, and the peak-seeking controller is applied to this model. The method is demonstrated in simulation using this simplified model.

I. Introduction

AS an airplane flies, it causes an upwash ahead of the wing and leaves a wake behind. This wake is characterized by the downwash behind the wing and by an accompanying upwash in the area on either side of the downwash region. By flying in the area of upwash, a second aircraft can gain a substantial efficiency boost because of the reduction in induced drag it will experience. This leads to the well-known fact that two aircraft flying in an appropriate formation can achieve overall efficiency much greater than were they flying separately.[1] This effect is analyzed using inviscid aerodynamic assumptions and lifting-line theory in Ref. 2, where it is noted that the effects were considered by Munk as early as 1919. The theory was put to test in actual aircraft by Hummel,[3] who established a fifteen per cent reduction on the second of a pair of civilian aircraft.

Because of the gains in efficiency, formation flight has been investigated as a way of increasing the range and duration of autonomous aerial vehicles. In Refs. 4 and 5, formations of several aircraft are considered, with the object of creating a solar-powered formation that could cruise at high altitude for arbitrarily long times. In Ref. 4, decentralized controllers are derived for a formation of five high-aspect-ratio craft and are shown to be capable of maintaining a prescribed formation despite the nonlinear, destabilizing moments induced on each plane by the aircraft ahead of it in the formation. The formation maintenance problem for a pair of F-16 class aircraft is considered in Ref. 6, though that paper relegates the rolling moments on the trailing craft to an inner-loop controller and considers only the lift and side force in designing an autopilot for the trailing plane.

In this paper, only a pair of aircraft is considered. The two craft can be thought of as a leader and a follower. The leader flies straight and level, as if alone. The second plane flies behind and outboard of the leader, in the upwash pattern on one side. (We will take it to be the right-hand side, but the analysis is the same for the left side.) In this configuration, there is only a negligible effect of the follower on the leader, and it is the follower that gets the direct benefit of reduced drag. The precise position of the follower for maximal drag reduction depends on the flight conditions and the geometries of the actual aircraft involved. For this reason, it is desirable to have a method of identifying the optimal location in flight. When considering unpiloted aerial vehicles, it is particularly important that this method be automated.

The general class of such control problems is that of peak-seeking control, also referred to as extremum-seeking control. Such problems were addressed as long ago as 1922 (Ref. 7) and are briefly reviewed in Ref. 8. More recently, the topic has been examined in connection with combustion instability in axial-flow compressors[9–11] and various other applications.[12] The analysis of these problems is addressed in Ref. 13, where an averaging framework is suggested.

In the next section, the aerodynamics of formation flight are briefly reviewed, using standard inviscid fluid theory, and a model of the effects of formation flight on the trailing aircraft is derived. The third section presents the peak-seeking scheme to be used to optimize the drag benefit during flight. Simulation results are presented in Sec. IV, and the fifth section concludes the paper.

II. Aerodynamics of Formation Flight

A detailed description of the aerodynamics of even a single aircraft is highly complicated. However, for the purposes of this discussion, most of the details of airflow over an airplane can be ignored. Instead, we take the point of view that the effects of flight on an aircraft, and of the aircraft on the air that flows over it, are principally caused by the wing and the creation of lift. For that reason, we will consider only the wing. Further, we will use the bound vortex model[1,2] to represent the wing of the leading craft. This will enable a straightforward model that captures the significant effects of formation flight on the trailing craft. This is not intended to be a complete and detailed model of the flow about the trailing craft. Also, because we assume inviscid and incompressible flow, the model loses its validity at near-transonic velocities.

As a further simplifying assumption, we will assume that the lead aircraft maintains straight and level flight at all times.

Received 8 March 2005; accepted for publication 10 October 2005.

*Assistant Professor, Mechanical and Aerospace Engineering. Senior Member AIAA.
†Professor, Mechanical and Aerospace Engineering. Fellow AIAA.
‡Visiting Undergraduate Student, Dipartimento di Elettronica ed Informatica.
§Associate Professor, Control and Instrumentation Engineering.

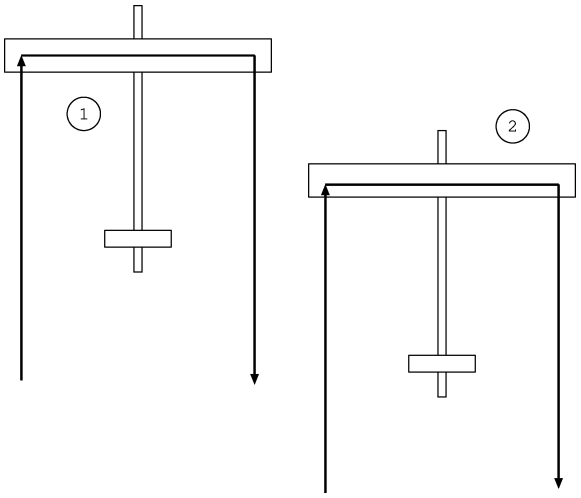

Fig. 1 Two aircraft in formation.

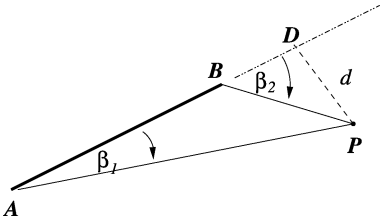

Fig. 2 Biot–Savart law.

A. Bound Vortex Model

Consider two aircraft flying in formation. Each craft is modeled using the horseshoe vortex, as in Fig. 1. This is intended to model the effects of the aircraft on the air around it, rather than to carefully model the airflow near the airplane itself. A central assumption in this model is that the effects on the airflow are almost entirely caused by the lift generated by the wing.

To calculate these effects, the wing is modeled as a single, straight vortex segment, which is "bound" to the wing. In keeping with the Helmholtz vortex laws, this vortex cannot simply end at the wing tips. Instead, it extends as a semi-infinite vortex from each wing tip. In general, these vortices are not fixed in space, but are free to move with the surrounding airmass. In the horseshoe vortex model, they are assumed to be straight, and under inviscid flow assumptions they lose none of their strength, regardless of how far away the wing becomes.

Remark 1: The vortex wake of an aircraft is of course much more complicated than this. In particular, most wings do not have a single, well-defined vortex from the wing tip. Instead, the vorticity is distributed through the wake behind the entire wing. Also, the wake descends slightly behind the aircraft. However, the majority of the vorticity, particularly from a wing with high aspect ratio, tends to be shed near the tip of the wing.

Remark 2: Because of the inviscid assumption on which the vortex model is based, there is naturally no dissipation in vortex strength with distance behind the lead craft. Although this is obviously incorrect for large distances, it is a good assumption at closer distances. In particular, because of the relatively low viscosity of air, small changes in the following distance have negligible effect on the strength of the vortex and its effect on the trailing airplane.

The velocity induced by a vortex segment on the surrounding inviscid fluid is described by the Biot–Savart law. The situation is shown in Fig. 2. In this figure, the velocity induced at the point P by the vortex segment running from A to B is given by

$$q = (\Gamma/4\pi d)(\cos\beta_1 - \cos\beta_2) \tag{1}$$

where Γ is the strength per unit length of the vortex and d is the shortest distance from P to the line along which the segment lies. The sign of the velocity is positive by the right hand rule about the vortex segment.

Applying this law to a single airplane explains the creation of the upwash ahead of a wing, the downwash behind, and the upwash regions outboard of each trailing vortex. When it is applied to Fig. 1, it is easy to see that there is little effect generated by the trailing aircraft on the leader. The upwash generated by the wing's bound vortex and that of the outboard wing-tip vortex decay too quickly to have any significant effect. And the inboard wing-tip vortex of the trailing plane is poorly positioned to have any effect. Similarly, the effect on the follower aircraft is seen to be almost entirely caused by the trailing vortex passing near the inboard wing tip. Because of these effects, we will consider only this vortex and its effect on the follower aircraft.

Remark 3: As noted in remark 1, the wake of an aircraft tends to descend as it leaves the wing. One of the results of formation flight is that the upwash ahead of a well-positioned follower tends to lift the portion of the wake that passes near the wing, so that as it passes the wing tip it is very nearly at the same altitude as the leading aircraft's wing tip.

In the formation shown in Fig. 1, the follower is entirely in an upwash region. This upwash causes the angle of attack along the wing to be greater than the nominal angle of attack of the aircraft itself, giving greater lift than would be otherwise generated. Because the upwash is inversely proportional to the distance from the vortex, the effect is strongest at the portion of the wing that is nearest the vortex and falls away sharply with distance. The result is that the majority of the lift induced on the trailing plane occurs near the end of its wing. This causes the craft to also experience a strong outward rolling moment.

The reduction in induced drag experienced by the follower craft is related to the lift created by the upwash field. Induced drag is a penalty of creating lift; the gain in efficiency can be thought of as result of the follower not having to create the lift itself and therefore not creating as much drag. The actual effect can be related to less downwash behind the wing.[14,15] Hummel[3] relates it to the lift vector on the wing itself, which is rotated forward as a result of the upwash. For our purposes it is enough to note that the gain in efficiency is related to the gain in lift. Thus, we can exchange the problem of minimizing drag with that of maximizing the vortex-induced lift on the follower craft.

Remark 4: A further effect of the upwash pattern on the follower wing is that the reduction in drag is greater near the end of the wing. This induces a small outward yawing moment on the follower craft. This is a minor effect.

Remark 5: Any side force induced on the follower is assumed negligible and will not be considered here.

Kutta–Joukowski Theorem: The strength of the vortices in the problem will be calculated using the Kutta–Joukowski theorem. [Joukowski (and its variations Joukovski and Joukowsky) is a Romanization of the name of N. E. Zhukovskiy, a Russian engineer born in 1847. The Romanized spelling is very common in the literature and is the one used in most of the references to this paper, and thus was chosen as the spelling to be used in the paper itself.] This theorem deals with the forces induced on a vortex fixed in space, caused by the motion of the surrounding fluid. Without derivation, the theorem can be presented as

$$\boldsymbol{F} = \rho \boldsymbol{V} \times \boldsymbol{\Gamma} \tag{2}$$

where ρ is the density of the fluid, $\boldsymbol{V}$ is the velocity of the fluid, and $\boldsymbol{\Gamma}$ is the strength per unit length of the bound vortex. The resulting force vector $\boldsymbol{F}$ is the force per unit length, imposed on the bound vortex. Applying this theorem to an aircraft in steady flight allows the computation of the strength of the bound vortex as

$$L = \rho V_\infty \Gamma b = W, \qquad \Rightarrow \qquad \Gamma = W/\rho V_\infty b \tag{3}$$

where L is the lift generated by the bound vortex, W the weight of the aircraft, V_∞ the velocity of the craft through the fluid, and b the wing span of craft. Thus the vortex strength is defined by the aircraft parameters and the default flight condition.

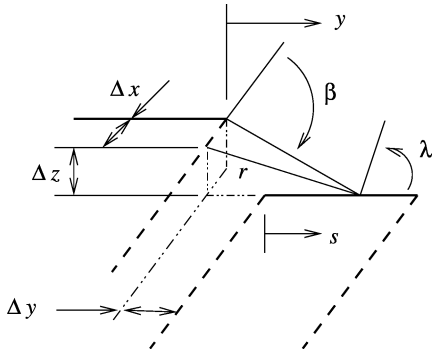

Fig. 3 Induced velocity at the trailing wing.

B. Computation of Induced Lift and Moment

The facts and assumptions of the last section will now be applied to the formation-flight problem described earlier. The geometry of the problem is shown in Fig. 3. The variables Δx, Δy, and Δz describe the location of the inboard wing tip of the trailing aircraft in relation to the outboard tip of the leader's wing; $\Delta x = \Delta y = \Delta z = 0$ results in the wing tips being aligned. The (constant) velocity of the lead plane is in the x direction, and the straight trailing vortex lies along the x axis.

We make three further simplifying assumptions. Because of the geometry of the situation, it is easy to see that a small change in following distance makes very little difference in the effects on the trailing plane; thus, we take this distance to be constant. For similar reasons, we take the trailing craft roll angle to be zero at all times and ignore any effect of sideslip.

Remark 6: Choosing the trailing aircraft roll angle to be zero requires that the trailing aircraft use roll control authority to cancel the moment induced by the lead craft and to use slideslip rather than roll to achieve small variations in lateral position. This is well within the capability of autopilot design. Because the necessary sideslip angles are expected to be small, and will come into the system as cosines, we ignore their effect in computing the effect of the upwash on the trailing aircraft. We expect that the errors in the model created by these assumptions will be small.

Under these assumptions, the problem reduces to computing the effects of a fixed vortex of known strength on the trailing wing. We do this by computing the upwash along the wing using the Biot–Savart law and from this computing the local angle of attack caused by upwash. Assuming a linear relation of lift to angle of attack, this allows the effects caused by the presence of the vortex to be added to the lift and moment generated by the orientation of the aircraft itself. Denoting the induced lift at a point on the wing as $\Delta L(s)$, we have the relation

$$d\Delta L(s) = \left[\rho V_\infty^2 c(s)/2\right] C_{L_\alpha}(s)\Delta\alpha(s)ds \tag{4}$$

Here, we use s to mean the point along the wing, with $s = 0$ being the inboard wing tip and $s = b$ the outboard wing tip. The chord at this point is $c(s)$, and $C_{L_\alpha}(s)$ denotes the local section lift-curve slope.

The incremental rolling moment induced is simply the incremental lift times the moment arm, giving

$$d\Delta M(s) = d\Delta L(s)(b/2 - s)ds \tag{5}$$

The induced angle of attack we will compute as

$$\Delta\alpha(s) = \tan^{-1}(w/V_\infty) \approx w/V_\infty \tag{6}$$

where w is the upwash velocity induced by the trailing vortex. We can compute this as $w = q\sin\lambda$, where λ is defined as in Fig. 3.

We can represent λ through the geometry of the situation as

$$\sin\lambda = \cos[\pi/(2 - \lambda)] = y/r = y\Big/\sqrt{y^2 + \Delta z^2} \tag{7}$$

with the distance r to the nearest point on the trailing vortex expressed as

$$r = \sqrt{y^2 + \Delta z^2} \tag{8}$$

The values of the cosines in Eq. (1) become

$$\cos\beta_1 = \frac{\Delta x}{\sqrt{\Delta x^2 + \Delta z^2 + (\Delta y + s)^2}} \qquad \text{and} \qquad \cos\beta_2 = -1 \tag{9}$$

where the second of these is caused by the assumption that the vortex extends to infinity behind the aircraft. Combining Eqs. (7), (8), and (9), and the Biot–Savart law gives

$$w(y) = q\sin\lambda = \frac{\Gamma}{4\pi}\frac{y}{y^2 + \Delta z^2}\left[1 + \frac{\Delta x}{\sqrt{\Delta x^2 + \Delta z^2 + (\Delta y + s)^2}}\right] \tag{10}$$

Assembling all of these results, we arrive at the expressions

$$\Delta L = \frac{\rho V_\infty \Gamma}{8\pi} C_{L_\alpha} \int_0^b \frac{yc(s)}{y^2 + \Delta z^2} \times \left[1 + \frac{\Delta x}{\sqrt{\Delta x^2 + \Delta z^2 + (\Delta y + s)^2}}\right] ds \tag{11}$$

and

$$\Delta M = \frac{\rho V_\infty \Gamma}{8\pi} C_{L_\alpha} \int_0^b \frac{yc(s)}{y^2 + \Delta z^2} \times \left[1 + \frac{\Delta x}{\sqrt{\Delta x^2 + \Delta z^2 + (\Delta y + s)^2}}\right] \left(\frac{b}{2 - s}\right) ds \tag{12}$$

where the lift-curve slope has been assumed constant for all s. For rectangular wings, the chord $c(s)$ is also constant, allowing further simplification.

The Biot–Savart result used so far becomes meaningless when the wing tip of the trailing aircraft approaches the core of the vortex. When $\Delta z = 0$ and $\Delta y + s = 0$ is included in the integration interval, in fact, the integral of ds/s is clearly unbounded and so would be the lift generated.

To deal with this, we note that the vortex core has finite diameter. Within this core, the velocity is often assumed to be linear with distance from the center of the core, and this will be assumed here. We can further simplify the equations by noting that Δx always has some appreciable value, while within the core y and Δz must both be small. Therefore, we take the value of $\cos\beta_1$ in this region to be 1. Combining these assumptions, the upwash within the core becomes simply

$$\bar{w} = k\sqrt{y^2 + \Delta z^2} \tag{13}$$

where the constant k is dependent on the vortex radius and strength and is computed such that the upwash is constant across the boundary of the vortex core. Using this approximation, the expressions for ΔL and ΔM become much simpler.

An example of the induced lift as a function of lateral and vertical separation is shown in Fig. 4. A zero value of separation refers to wing tips aligned. The figure was generated using values taken from Ref. 16 for a Cessna-172 type aircraft. The vortex core radius was chosen such that at the edge of the core the induced angle of attack is approximately 12 deg; above this value the total angle of attack is such that the wing would most likely stall. This value was chosen because if the wing stalls the assumptions on which the preceding aerodynamic model is based become invalid. The actual value used is 6.9 in., which is about 1.5% of the wing span. This is a small value (see remark 7), and as the lift function becomes better behaved as the core radius increases, this can be considered a worst case within the assumptions made and is reasonable given experimental data. Note that without further information about vortex behavior for a specific wing, actual values cannot be deduced. As

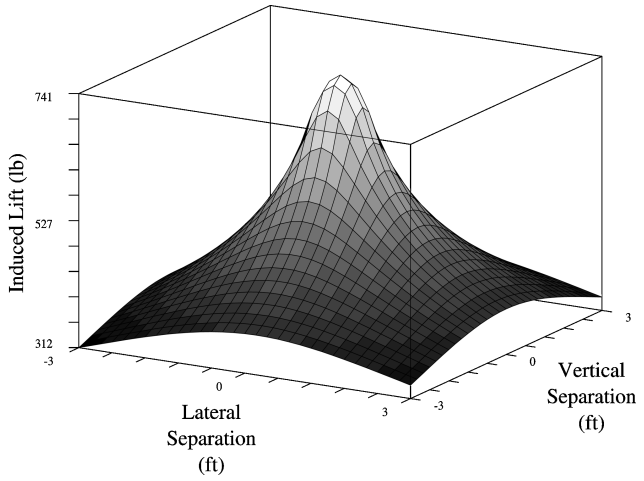

Fig. 4 Induced lift.

this paper explores the utility of peak-seeking control in this context, a representative rather than exact value for the radius will suffice.

Remark 7: The horseshoe vortex is a very simplified model of the wake behind an aircraft. However, when a nonzero core radius for the trailing vortex is included, it conforms very well to a more complex vortex-lattice model[17]; the reference notes results for a radius of 3% of the span when modeling unswept wings with taper ratio 8. In particular, when considering both formation-induced lift and moment as a function of lateral position, the horseshoe vortex agrees with the general shape of the curves produced by the more complex model, though the location of the peaks of these curves is slightly off. Later wind-tunnel experiments[18] indicate that vortex lattice results mimic experimental results quite well.

C. Estimation of Drag Reduction

The reduction in drag in formation flight is caused by the reduction of induced drag. Katz and Plotkin[15] describe induced drag as being caused by the rotation of the lift vector rearwards as a result of wake-induced downwash behind the wing. Following this decription, the reduction in induced drag caused by formation flight can be expressed as the rotation forward of the lift vector along the wing of the trailing aircraft as a result of the upwash caused by the wake of the lead vehicle.

Following this logic, we see that the reduction in drag is, like the increase in lift, related directly to the angle $\Delta\alpha$ described by Eq. (6). We can write

$$dD_i(s) = -dL(s)\Delta\alpha(s) \tag{14}$$

where $dL(s)$ is the local value of lift along the incremental span length ds and the integral of this value over the span is the total lift on the vehicle. Evaluating the integral would require knowing the lift distribution, which is dependent on the wing shape and local flow. Hummel[3] makes the approximation

$$\Delta D_i = -L(\bar{w}/V_\infty) \tag{15}$$

where $\bar{w}$ is the average value of formation-induced upwash and L is the total lift.

Note that the change in lift distribution caused by control surface deflection, necessary to counter the formation-induced roll moment, does not affect the computation of additive lift above because the induced lift adds to whatever lift is already being created. However, the lift distribution is important in the calculation of induced drag; the larger forward rotation of the lift at one end as a result of large values of upwash is balanced by the lack of much upwash on the other end of the wing, where a roughly equivalent amount of lift must be generated to balance the roll moment.

Because the average value $\bar{w}/V_\infty$ represents a change in the overall body angle of attack, we estimate our drag reduction as

$$\Delta D_i = L\,\Delta\alpha_{\text{body}} \tag{16}$$

where $\Delta\alpha_{\text{body}}$ is any change in the overall body angle of attack caused by formation effects.

D. Effects of Wing Geometry and Follower Position

Although the topic of this paper is control rather than aerodynamics, a few comments on the effects of wing geometry and follower position are in order. The effect of the second of these is straightforward; the effect of the first is less so. In both cases, the effects are because of the combination of upwash outboard of the leading wing's vortex wake and the strong downwash just inside.

First consider an aircraft with a rectangular wing, such as sketched in Fig. 1, and let the trailing vortex from the leader be fixed in space. (Let the vortex have some finite diameter, so that the induced velocities remain finite.) As the follower craft gets farther from the vortex, both the lift and moment induced on it go to zero. As it comes closer, both lift and moment increase, until both are maximized as the wing tip touches the vortex. Should the follower continue inward, so that its wing tip is now in the downwash field, both lift and moment begin to decrease. This is because the downwash creates a downward force on the wing and thus a moment in the opposite direction to that imposed on the rest of the wing. As this section has the greatest moment arm, the reduction in moment is larger (in proportion to the overall induced moment) than is the reduction in lift. This asymmetry can be seen near the vortex by comparing the moment function displayed in Fig. 5 with the lift function in Fig. 4. As more of the wing enters the downwash area, there comes a point at which there is still positive induced lift, while the moment goes to zero. The extreme case occurs when the vortex runs down the centerline of the follower craft. Were this case physically possible, it would result in zero overall induced lift, while a moment rolling the follower into the leader's wake would be at maximum strength.

If we replace the rectangular wing on the follower craft with a delta wing, the effects on the follower become less straightforward. In this case, a small overlap of the follower craft, so that a wing tip is in the downwash region, might be desirable. This is because the area of the wing section in downwash is small, while the part of the wing now in the strong upwash section has a larger chord [consider Eq. (4)]. Therefore, the net effect is a gain in lift. The greater moment arm of the section in the downwash region exaggerates the effect on the total induced moment, however. Because of this, the moment will begin to decrease even as the lift continues to increase with overlap. This effect is illustrated in Fig. 6, which shows the effect on a trailing aircraft with a delta wing. The lateral position varies from $-b/2$, so that the vortex runs down the follower centerline, to $b/2$. Note that the point of maximum induced lift coincides with an overlap of approximately $0.15b$, while the maximum induced moment remains near zero overlap.

Because many aircraft have at least some taper to their wings, even in this simplified analysis the optimal flight formation would include some overlap. When the effect of a distributed vortex wake from a leading craft with wing taper is included, the overlap for maximum lift can be quite high.

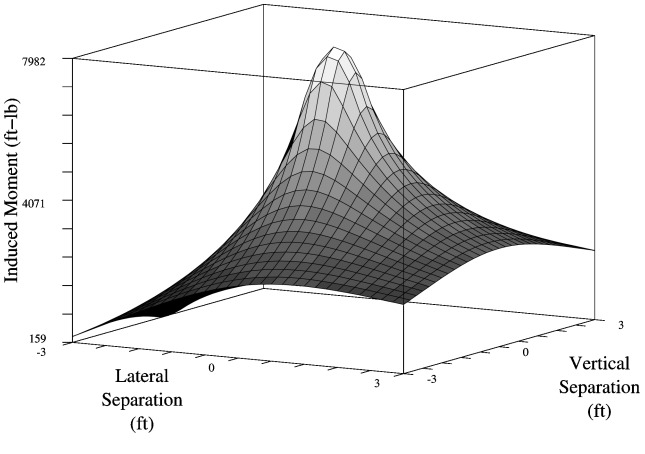

Fig. 5 Induced moment function.

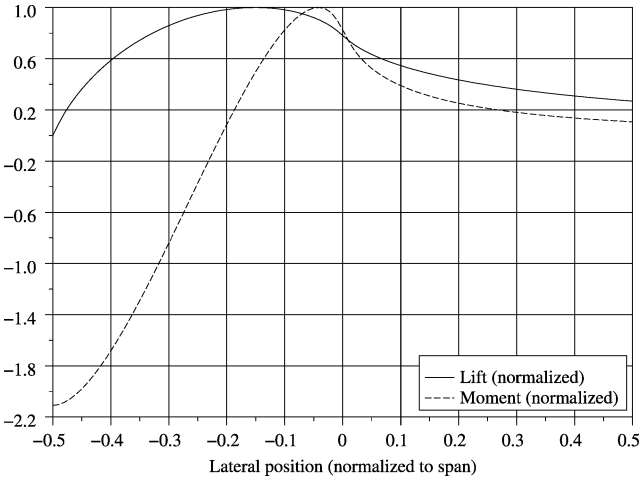

Fig. 6 Normalized lift and moment vs lateral position for a delta wing.

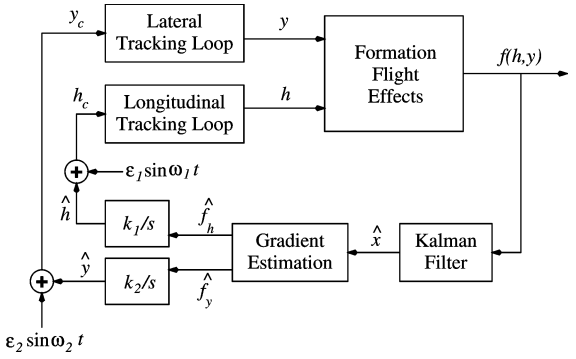

Fig. 7 Block diagram of peak-seeking controller.

Remark 8: All of the analysis in this paper ignores the changes in lift distribution on the follower aircraft wing as a result of control deflections. It is known[3] that this can have an effect on the drag reduction. (Hummel reports an enhancement.) However, this effect is specific to particular aircraft and will not be addressed here. It can be taken as a further reason that the precise position for greatest drag reduction is unlikely to be known in advance.

III. Peak-Seeking Scheme

The physical problem having been defined, we proceed to derive a controller to maximize the lift during flight. As demonstrated, the lift is primarily a function of the lateral and vertical separation of the aircraft, and as modeled this is specifically true. Thus, we seek a controller that optimizes online a nonlinear function of the system states Δy and Δz. The structure of the resulting controller will be as shown in Fig. 7.

The peak-seeking scheme begins with the proposition that the current value of the states is the optimum. Were this true, the control system would be primarily concerned with maintaining these values; this is the usual disturbance-rejection task. To find out if it is true, a dither signal is added to each of the states of interest. The aircraft tracks these oscillating states, and the resulting motion of the aircraft results in an oscillation in the value of the function to be maximized.

The value of the function is fed to a modified Kalman filter, which is used to estimate both the values of the gradients of the function with respect to the states of interest and the mean value of the function (the value with the oscillation subtracted). The estimated gradients are used as input for the controller, which uses them to adjust the position of the vehicle to increase the mean value. The loop continues until the gradients are estimated to be zero, at which point the optimum is considered to be reached. Depending on the application, the peak-seeking aspect of the controller might be turned off at this point. Often, as here, it will be left active, to ensure that the system does not drift from the optimum, or that disturbances are rejected.

In most earlier work (for example, Ref. 9), only the sign of the estimated gradient is used in the peak-seeking loop; to the authors' knowledge, the first use of the gradient estimate itself in the loop is presented in Ref. 19.

Remark 9: The peak-seeking approach here is not an attempt to model the nonlinear effects of the trailing vortex. Such an approach might assume some form for the effects and use a neural net to approximate the values of the parameters that describe the assumed model. Broadband excitation might also be better suited to estimating the properties of a model dependent on several parameters. Once a model of the effects was obtained, it could be used to optimize the position of the trailing aircraft.

Instead, the approach outlined here uses only local information and chooses a modification of the operating point that will increase the value of the function. This does not require any predetermined assumed form of the function being maximized and requires only two values be estimated (the two elements of the gradient); in general, if the system is optimizing over m variables, m values will have to be estimated. Note that because of the form of the filter to be derived distinct dither frequencies are assumed.

We will first derive a Kalman filter to be used to derive the gradient and then implement a control loop that includes the filter.

A. Kalman Filter for Gradient Estimation

Because we are assuming straight and level flight on the part of the lead aircraft, we can ignore that craft in deriving the filter and the controller. Therefore, we will define the function to be maximized as a function of the trailing aircraft states only. In this section, we use h to denote the altitude of the aircraft, rather than $-z$. The variable z is taken to be the measurement of the linear system under consideration.

We begin by expanding the function to be extremized as

$$f(h, y) = f(\hat{h}, \hat{y}) + f_h(\hat{h}, \hat{y})\delta h + f_y(\hat{h}, \hat{y})\delta y + o(\delta h, \delta y) \quad (17)$$

where $(\hat{h}, \hat{y})$ is the current estimate. Introducing the dither signals into the input of the tracking loop (see Fig. 7), the output is assumed to firstorder to be

$$h \cong \hat{h} + \delta h = \hat{h} + \bar{\varepsilon}_1 \sin(\omega_1 t + \theta_1) \quad (18)$$

$$y \cong \hat{y} + \delta y = \hat{y} + \bar{\varepsilon}_2 \sin(\omega_2 t + \theta_2) \quad (19)$$

The underlying assumptions are that the gradient changes are slow with respect to the tracking loops and the dither frequencies, so that $\hat{h}$ and $\hat{y}$ can be assumed constant and that the dither inputs are tracked well, except for an amplitude and phase uncertainty. Under these assumptions, the expansion (17) of the formation-flight effects becomes

$$f(h, y) = f(\hat{h}, \hat{y}) + \bar{\varepsilon}_1 f_h(\hat{h}, \hat{y}) \sin[\omega_1 t + \theta_1(t)] + \bar{\varepsilon}_2 f_y(\hat{h}, \hat{y}) \sin[\omega_2 t + \theta_2(t)] + o(\delta h, \delta y) \quad (20)$$

where $\varepsilon_{()}$ and $\omega_{()}$ of the input dither signal are to be chosen by the designer.

To estimate the two gradients using the Kalman filter, we define the state variables

$$x \equiv \begin{bmatrix} x_1 \\ x_2 \\ x_3 \\ x_4 \\ x_5 \end{bmatrix} = \begin{bmatrix} \tilde{f}_h \sin(\omega_1 t + \theta_1) \\ \tilde{f}_h \cos(\omega_1 t + \theta_1) \\ \tilde{f}_y \sin(\omega_2 t + \theta_2) \\ \tilde{f}_y \cos(\omega_2 t + \theta_2) \\ f(\hat{h}, \hat{y}) \end{bmatrix} \quad (21)$$

where $\tilde{f}_h = \bar{\varepsilon}_1 f_h(\hat{h}, \hat{y})$ and $\tilde{f}_y = \bar{\varepsilon}_2 f_y(\hat{h}, \hat{y})$. We act for now as if the pair $(\hat{h}, \hat{y})$ were fixed, so that f, f_h, and f_y can be treated as unknown constants. Furthermore, we assume that θ_1 is a Brownian motion process with zero mean and variance $E[\theta_1(t)\theta_1(\tau)] = \sigma_1^2 t$ if

$\tau \geq t$ (with similar assumptions on θ_2). This fits the theory given in Ref. 20. If the Îto differentials of x are taken, then we get

$$\mathrm{d}x = Fx\,\mathrm{d}t + \mathrm{d}Gx + \mathrm{d}w \tag{22}$$

where

$$F = \begin{bmatrix} -\frac{\sigma_1^2}{2} & \omega_1 & 0 & 0 & 0 \\ -\omega_1 & -\frac{\sigma_1^2}{2} & 0 & 0 & 0 \\ 0 & 0 & -\frac{\sigma_2^2}{2} & \omega_2 & 0 \\ 0 & 0 & -\omega_2 & -\frac{\sigma_2^2}{2} & 0 \\ 0 & 0 & 0 & 0 & \kappa \end{bmatrix}$$

$$\mathrm{d}G = \begin{bmatrix} 0 & \mathrm{d}\theta_1 & 0 & 0 & 0 \\ -\mathrm{d}\theta_1 & 0 & 0 & 0 & 0 \\ 0 & 0 & 0 & \mathrm{d}\theta_2 & 0 \\ 0 & 0 & -\mathrm{d}\theta_2 & 0 & 0 \\ 0 & 0 & 0 & 0 & 0 \end{bmatrix}$$

$$\mathrm{d}w = \begin{bmatrix} 0 & 0 & 0 & 0 & \mathrm{d}w_0 \end{bmatrix}^T$$

where $w_0(t)$ is a white Gaussian process noise with zero mean and spectral density W_0, and the values for σ_1, σ_2, κ, and W_0 are empirically determined through simulation and filter performance.

Allowing the higher-order terms in Eq. (20) to be considered as noise, the measurement equation is expressed as

$$\begin{aligned} z(t) &= [1 \quad 0 \quad 1 \quad 0 \quad 1]x(t) + v(t) \\ &= Hx(t) + v(t) \end{aligned} \tag{23}$$

where $v(t) \sim N[0, V(t)]$, and $z(t)$ recovers $f(\hat{h}, \hat{y})$.

The filter for the preceding dynamic structure (22) and (23) is taken to be the best linear minimum variance estimator as

$$\dot{\hat{x}} = F\hat{x} + K(z - \hat{z}) \tag{24}$$

where

$$K = PH^TV^{-1} \tag{25}$$

and P satisfies the Riccati equation

$$\dot{P} = FP + PF^T + \Delta(X) + W - PH^TV^{-1}HP \tag{26}$$

where X is the variance of x taken here to be in steady state X_{ss}. Therefore, the sum $\Delta(X_{\mathrm{ss}}) + W$, where W is the variance of the additive noise, is

$$\Delta(X_{\mathrm{ss}}) + W = \begin{bmatrix} \sigma_1^2 & 0 & 0 & 0 & 0 \\ 0 & \sigma_1^2 & 0 & 0 & 0 \\ 0 & 0 & \sigma_2^2 & 0 & 0 \\ 0 & 0 & 0 & \sigma_2^2 & 0 \\ 0 & 0 & 0 & 0 & W_0 \end{bmatrix} \tag{27}$$

The estimates of state associated with altitude are

$$\hat{x}_1 = \tilde{f}_h \sin(\widehat{\omega_1 t} + \theta), \qquad \hat{x}_2 = \tilde{f}_h \cos(\widehat{\omega_1 t} + \theta) \tag{28}$$

We can obtain the magnitude of the gradient as

$$|\hat{\tilde{f}}_h| = \sqrt{\hat{x}_1^2 + \hat{x}_2^2} \tag{29}$$

Combining Eqs. (28) and (29), the gradient $\tilde{f}_h$ is estimated as

$$\hat{\tilde{f}}_h = \sqrt{\hat{x}_1^2 + \hat{x}_2^2}\,\mathrm{sgn}(\hat{x}_1 \sin\omega_1 t + \hat{x}_2 \cos\omega_1 t) \tag{30}$$

Similarly, the gradient $\tilde{f}_y$ is computed as

$$\hat{\tilde{f}}_y = \sqrt{\hat{x}_3^2 + \hat{x}_4^2}\,\mathrm{sgn}(\hat{x}_3 \sin\omega_2 t + \hat{x}_4 \cos\omega_2 t) \tag{31}$$

Note that because of the signum function, the gradient estimates are not necessarily continuous. Note also that $\bar{\varepsilon}_1$ and $\bar{\varepsilon}_2$ are embedded in Eqs. (30) and (31). Their effect is compensated by the values of the gains k_1 and k_2 chosen in the peak-seeking loop in Fig. 7.

B. Sinusoidal Tracking Loop for Aerodynamics

For the purpose of control system design, the aircraft's dynamics are frequently linearized about some operating condition or flight regime. The control surfaces and engine thrust are trimmed at these conditions, and the control system is designed to maintain them, that is, to force any perturbation from these conditions to zero.

Also, it is customary to separate the longitudinal motion from the lateral motion in studying small perturbations from trim conditions. In most cases the lateral and longitudinal dynamics are only lightly coupled, and the control system can be designed for each channel without regard to the other.[21] This approach is taken in this work, so that the longitudinal and lateral tracking loops are designed separately. The state vectors, plant, and control matrices used are as follows:

1) Longitudinal dynamics:

$$\begin{bmatrix} \dot{s} \\ \dot{\alpha} \\ \dot{q} \\ \dot{\theta} \\ \dot{h} \end{bmatrix} = \begin{bmatrix} X_s & X_\alpha & 0 & -g & 0 \\ Z_{sV} & Z_{\alpha V} & 1 & 0 & 0 \\ M_s & M_\alpha & M_q & 0 & 0 \\ 0 & 0 & 1 & 0 & 0 \\ 0 & -V & 0 & V & 0 \end{bmatrix} \begin{bmatrix} s \\ \alpha \\ q \\ \theta \\ h \end{bmatrix} + \begin{bmatrix} X_E \\ Z_{\mathrm{EV}} \\ M_E \\ 0 \\ 0 \end{bmatrix} \delta_E + \begin{bmatrix} \alpha \\ -1/V \\ 0 \\ 0 \\ 0 \end{bmatrix} \bar{L} \tag{32}$$

where

s	=	change in speed, ft/s
α	=	angle of attack, rad
q	=	pitch rate, rad/s
θ	=	pitch angle, rad
h	=	altitude,ft
δ_E	=	elevator deflection, rad

2) Lateral dynamics:

$$\begin{bmatrix} \dot{\beta} \\ \dot{p} \\ \dot{r} \\ \dot{\phi} \\ \dot{\psi} \\ \dot{y} \end{bmatrix} = \begin{bmatrix} Y_{\beta V} & Y_{\mathrm{pV}} & Y_{\mathrm{rV}} - 1 & gV & 0 & 0 \\ L_\beta & L_p & L_r & 0 & 0 & L_y \\ N_\beta & N_p & N_r & 0 & 0 & 0 \\ 0 & 1 & 0 & 0 & 0 & 0 \\ 0 & 0 & 1 & 0 & 0 & 0 \\ -V & 0 & 0 & 0 & V & 0 \end{bmatrix} \times \begin{bmatrix} \beta \\ p \\ r \\ \phi \\ \psi \\ y \end{bmatrix} + \begin{bmatrix} Y_{\mathrm{AV}} & Y_{\mathrm{RV}} \\ L_A & L_R \\ N_A & N_R \\ 0 & 0 \\ 0 & 0 \\ 0 & 0 \end{bmatrix} \begin{bmatrix} \delta_A \\ \delta_R \end{bmatrix} + \begin{bmatrix} 0 \\ 1 \\ 0 \\ 0 \\ 0 \\ 0 \end{bmatrix} \bar{L}_u \tag{33}$$

where

β = sideslip angle, rad
p = roll rate, rad/s
r = yaw rate, rad/s
ϕ = roll angle, rad
ψ = yaw angle, rad
y = cross-track displacement, ft
δ_A = aileron deflection, rad
δ_R = rudder deflection, rad

Note the additions to the usual linear aircraft equations. The longitudinal channel includes an additional input to the $\dot{\alpha}$ equation, as a result of the vortex-induced lift. For the same of controller design, this is modeled as a constant input. The lateral channel [Eq. (33)] includes both a constant term and a linearly varying term in the $\dot{p}$ equation, this time caused by the vortex-induced rolling moment.

Because the command input of the system is oscillatory, Eqs. (32) and (33) cannot be used directly to derive the controllers. First, an error state that maps the oscillatory system into a linear space, in which the system does not appear oscillatory, must be developed. Standard linear-quadratic-regulator (LQR) techniques can then be used to derive the controller. Note that, for state space, a similar approach was seen in Ref. 21. The design process for the controller for the longitudinal states will be covered briefly here.

First, an error state is defined as

$$e = h_c - h \tag{34}$$

and, taking derivatives and substituting values from Eq. (32), this leads to the equations

$$e_1 = e = h_c - h = \hat{h} + \varepsilon_1 \sin\omega_1 t - h$$

$$e_2 = \dot{e}_1 = \dot{h}_c - \dot{h} = \omega_1 \varepsilon_1 \cos\omega_1 t - V(\theta - \alpha)$$

$$e_3 = \dot{e}_2 = -\omega_1^2 \varepsilon_1 \sin\omega_1 t - V(\dot{\theta} - \dot{\alpha})$$

Now, this third error state has the derivative

$$\dot{e_3} = -\omega_1^2 e_2 + V\left(\omega_1^2\alpha + \ddot{\alpha}\right) - V\left(\omega_1^2\theta + \ddot{\theta}\right)$$

The repetition of terms such as $\omega_1^2\alpha + \ddot{\alpha}$ leads us to introduce the new state

$$\bar{\theta} = \omega_1^2\theta + \ddot{\theta}$$

which has the derivative

$$\dot{\bar{\theta}} = \omega_1^2\dot{\theta} + \theta^{(3)} = \omega_1^2 q + \ddot{q}$$

Following in this pattern, we introduce the states

$$\bar{\alpha} = \omega_1^2\alpha + \ddot{\alpha}, \qquad \bar{s} = \omega_1^2 s + \ddot{s}, \qquad \bar{q} = \omega_1^2 q + \ddot{q}$$

and the control variable

$$\bar{\delta}_E = \omega_1^2\delta_E + \ddot{\delta}_E \tag{35}$$

Using these states and control, the dynamic system from Eq. (32) becomes

$$\begin{bmatrix} \dot{e}_1 \\ \dot{e}_2 \\ \dot{e}_3 \\ \dot{\bar{s}} \\ \dot{\bar{\alpha}} \\ \dot{\bar{q}} \\ \dot{\bar{\theta}} \end{bmatrix} = \begin{bmatrix} 0 & 1 & 0 & 0 & 0 & 0 & 0 \\ 0 & 0 & 1 & 0 & 0 & 0 & 0 \\ 0 & -\omega^2 & 0 & 0 & V & 0 & -V \\ 0 & 0 & 0 & X_s & X_\alpha & 0 & -g \\ 0 & 0 & 0 & Z_{\mathrm{sv}} & Z_{\alpha V} & 1 & 0 \\ 0 & 0 & 0 & M_s & M_\alpha & M_q & 0 \\ 0 & 0 & 0 & 0 & 0 & 1 & 0 \end{bmatrix} \begin{bmatrix} e_1 \\ e_2 \\ e_3 \\ \bar{s} \\ \bar{\alpha} \\ \bar{q} \\ \bar{\theta} \end{bmatrix} + \begin{bmatrix} 0 \\ 0 \\ 0 \\ X_E \\ Z_E \\ M_E \\ 0 \end{bmatrix} \bar{\delta}_E \tag{36}$$

Note that the new control variable $\bar{\delta}_E$ is not oscillatory; a glance at Eq. (35) shows that the actual control δ_E will, however, have the desired sinusoidal characteristics.

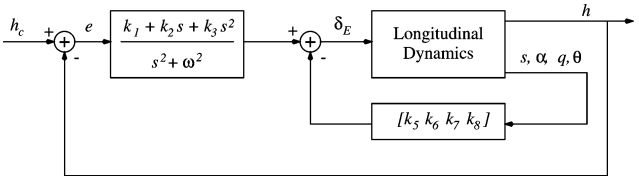

Fig. 8 Longitudinal channel controller.

Now that a standard linear system has been derived, standard LQR techniques quickly provide a stable controller for this system. Converting the states and control back to the original state-space results in a controller of the form in Fig. 8.

For the lateral dynamics we have

$$\begin{bmatrix} \dot{e}_1 \\ \dot{e}_2 \\ \dot{e}_3 \\ \dot{e}_4 \\ \dot{\bar{\beta}} \\ \dot{\bar{p}} \\ \dot{\bar{r}} \\ \dot{\bar{\phi}} \\ \dot{\bar{\psi}} \\ \dot{\bar{\xi}} \end{bmatrix} = \begin{bmatrix} 0 & 1 & 0 & 0 & 0 & 0 & 0 & 0 & 0 & 0 \\ 0 & 0 & 1 & 0 & 0 & 0 & 0 & 0 & 0 & 0 \\ 0 & 0 & 0 & 1 & 0 & 0 & 0 & 0 & 0 & 0 \\ 0 & 0 & -\omega^2 & 0 & V & 0 & 0 & 0 & -V & 0 \\ 0 & 0 & 0 & 0 & Y_{\beta V} & Y_{\mathrm{pV}} & Y_{\mathrm{rV}} - 1 & g_V & 0 & 0 \\ 0 & -\omega L_y & 0 & -L_y & L_\beta & L_p & L_r & 0 & 0 & 0 \\ 0 & 0 & 0 & 0 & N_\beta & N_p & N_r & 0 & 0 & 0 \\ 0 & 0 & 0 & 0 & 0 & 1 & 0 & 0 & 0 & 0 \\ 0 & 0 & 0 & 0 & 0 & 0 & 1 & 0 & 0 & 0 \\ 0 & 0 & 0 & 0 & 0 & 0 & 0 & 1 & 0 & 0 \end{bmatrix}$$

$$\times \begin{bmatrix} e_1 \\ e_2 \\ e_3 \\ e_4 \\ \bar{\beta} \\ \bar{p} \\ \bar{r} \\ \bar{\phi} \\ \bar{\psi} \\ \bar{\xi} \end{bmatrix} + \begin{bmatrix} 0 & 0 \\ 0 & 0 \\ 0 & 0 \\ 0 & 0 \\ Y_{\mathrm{AV}} & Y_{\mathrm{RV}} \\ L_A & L_R \\ N_A & N_R \\ 0 & 0 \\ 0 & 0 \\ 0 & 0 \end{bmatrix} \begin{bmatrix} \bar{\delta}_A \\ \bar{\delta}_R \end{bmatrix} \tag{37}$$

where

$$e_1 = y_c - y, \qquad y_c = y_0 + \varepsilon \sin\omega t, \qquad e_2 = \dot{e}_1, \qquad e_3 = \dot{e}_2$$

$$e_4 = \dot{e}_3, \qquad \bar{\beta} = \omega^2\dot{\beta} + \beta^{(3)}, \qquad \bar{p} = \omega^2\dot{p} + p^{(3)}$$

$$\bar{r} = \omega^2\dot{r} + r^{(3)}, \qquad \bar{\phi} = \omega^2\dot{\theta} + \theta^{(3)} = \dot{\xi}, \qquad \bar{\psi} = \omega^2\dot{\psi} + \psi^{(3)}$$

$$\xi = \omega^2\theta + \phi^{(3)}, \qquad \bar{\delta}_A = \omega^2\dot{\delta}_A + \delta_A^{(3)}, \qquad \bar{\delta}_R = \omega^2\dot{\delta}_R + \delta_R^{(3)}$$

and again, LQR techniques provide a stable controller for the system. In these dynamics, the rolling moment caused by the vortex is included, as it is a very strong term. This led to the need for one higher level of differentiation in the error states.

C. Peak-Seeking Loop

The controller derived in the preceding section assumes a constant value to track, in keeping with the assumption that the estimate of the optimal flight position changes slowly. Note that this assumption is inherent in the timescale separation that allows a dither signal to be imposed on a "constant" nominal value of $(\hat{y}, \hat{h})$ in the Kalman filter.

Given that the initial assumption of $(\hat{y}, \hat{h})$ is bound to be incorrect, we must have a way to update it. In some earlier work,[10] where only the sign of the gradient was found, this was done merely by integrating a constant times the sign of the estimated gradient. Later,[19] this was extended to integrating a multiple of the gradient estimate itself. The second approach will be used here, giving an overall control loop as shown in Fig. 7.

IV. Simulation Results

In this section, we apply the peak-seeking controller derived in Sec. III to the formation flight problem. Rather than attempt to minimize drag directly, we instead maximize the rolling moment induced by the vortex from the lead craft. Recall that for the aircraft geometry under consideration, this maximum corresponds to the maximum induced lift. Although drag is difficult if not impossible to measure directly, the induced moment can easily be estimated through its effects on the aircraft dynamics. Hummel[3] simply maximizes steady-state aileron deflection; this is a good proxy for induced moment if sideslip is controlled to zero. More generally, given that the control deflections are known, and the states and accelerations of the aircraft known (at least to a good approximation), then the portion of acceleration caused by added moment should be easily approximated. We assume for this simulation that the moment can be effectively measured.

For the puposes of simulation, the lift and moment induced by the vortex are computed as in Sec. II.B and added to a linear aircraft model. The model chosen is aircraft A from Ref. 16, which is much like the Cessna-172 general-aviation aircraft. The aircraft parameters and nominal flight condition are given as

$$V_\infty = 219\,\text{ft/s}, \qquad h = 5000\,\text{ft}, \qquad \rho = 0.002050\,\text{sl/ft}^3$$

$$W = 2645\,\text{lb}, \quad b = 35.8\,\text{ft}, \quad c = 4.9\,\text{ft}$$

Using Eq. (3), this provides the strength per unit length for all vortices to be

$$\Gamma = \frac{2645}{219(0.00205)(35.8)} = 164.6\,\text{ft}^2/\text{s}$$

We are also given a lift coefficient slope for the aircraft. This is an overall coefficient; the airfoil slope is likely to be higher. The theoretical C_{L_α} for any thin airfoil is 2π per radian; experience indicates that a value of about 5.5 per radian is more accurate. The listed overall C_{L_α} of 4.6 is somewhat less. As the upwash affects primarily the airfoil, a value of 5.5 is reasonable. All other values are as given in Ref. 16.

Time histories from a simulation with initial condition $[h(0), y(0)] = (3, 3)$ are given. The optimal position for this geometry is $(0, 0)$. The initial estimate of the optimal position is, however, the initial condition. The gradient estimates are initialized to zero, and the moment estimate is initialized to the initial measurement of the moment. The controls begin at their nominal values, that is, the aircraft is not trimmed for flight in formation, but for lone flight. Also, the initial angle of attack is that for lift equal weight without the presence of the trailing vortex (given as zero in Ref. 16); note that this means that the vehicle is actually generating much more lift than necessary, as this initial condition does not account for the additional lift caused by the nearby vortex. This set of results is generated assuming zero error in the measurement of the induced moment. The dither frequencies ω_1 (altitude dither) and ω_2 (lateral position dither) are 2 and 1 rad/s, respectively. These values are not tuned for optimal performance; they were merely checked to be certain that the frequencies are well within the response of the airframe. Fine tuning these frequencies could likely improve the performance of the controller.

The position, command, and gradient estimates are presented for the vertical channel in Fig. 9 and for the lateral channel in Fig. 10. The control commands and the coordinates show the expected oscillatory nature. The craft converges to the optimal position in approximately 80 s, after which the gradient estimates oscillate about zero. Note the discontinuous nature of the estimate in the vertical channel; this can be traced to the signum function in the estimate calculation.

The estimated and actual values of the moment are plotted in Fig. 11. The effect of both dither signals on the moment can be seen in the oscillating measured moment. The moment estimate tracks the actual moment well, with the expected slight delay. The best indication of the benefits of formation flight is in Fig. 12, which shows the angle of attack. There are immediate large transients as

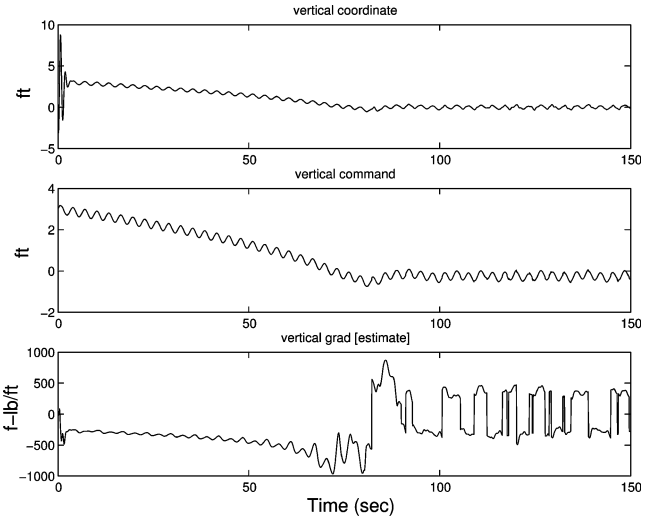

Fig. 9 Results for altitude channel.

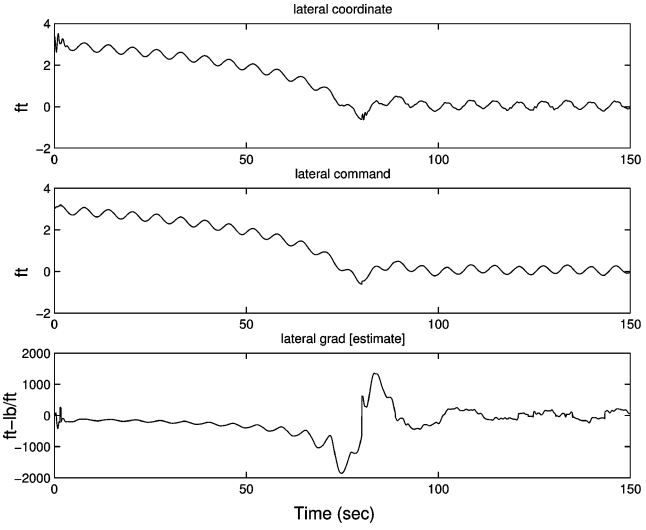

Fig. 10 Results for lateral channel.

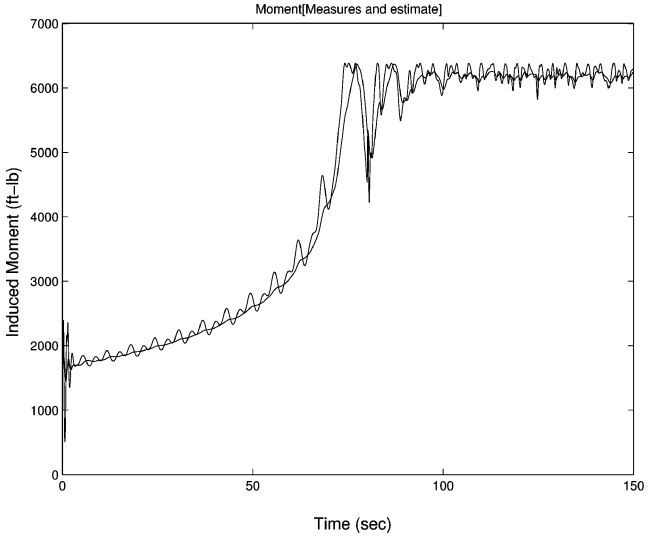

Fig. 11 Moment and moment estimate vs time.

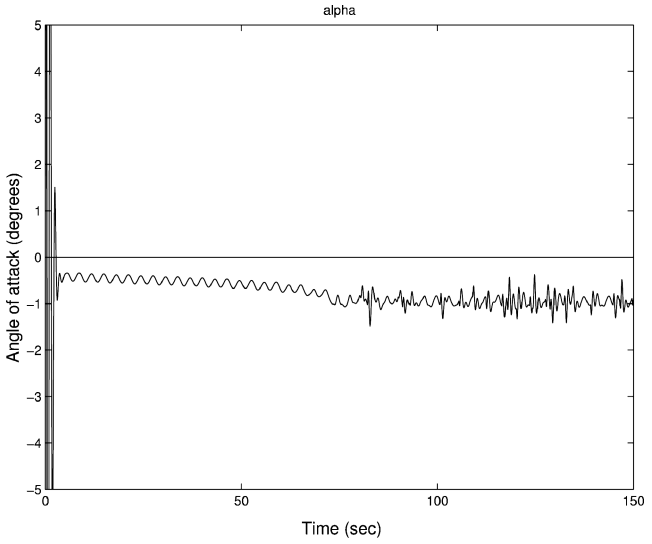

Fig. 12 Angle of attack vs time.

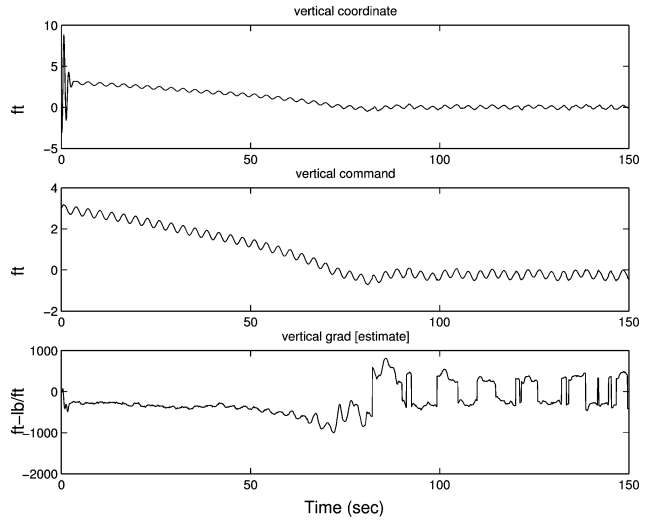

Fig. 13 Results for altitude channel, with measurement noise.

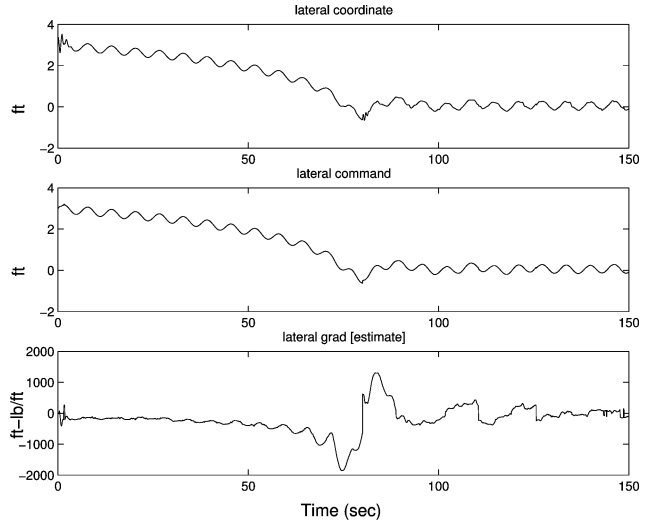

Fig. 14 Results for lateral channel, with measurement noise.

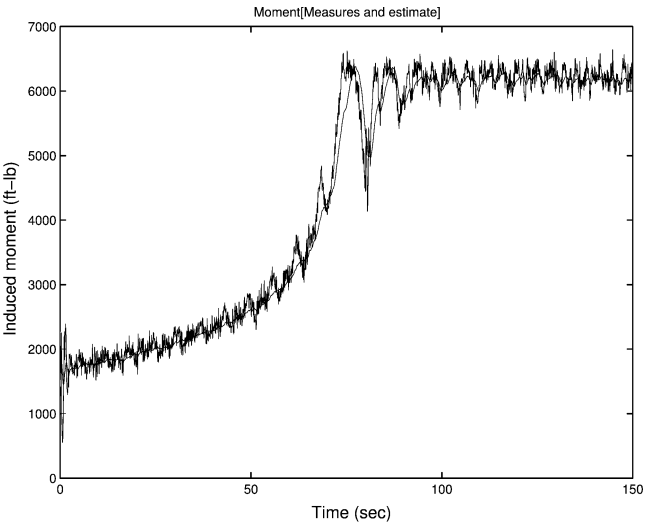

Fig. 15 Moment and moment estimate, with measurement noise.

the controller trims for the vortex-induced lift at the initial position. These disappear rapidly, after which α is seen to steadily decrease, finally hovering around a value of nearly -1 deg. This represents a reduction in the body angle of attack away from the nominal, caused by the additional lift from the lead aircraft vortex. This is because of the need to generate less lift through body angle and implies a corresponding reduction in induced drag. We approximate this reduction from Eq. (16) and the given weight of the aircraft to be about $\Delta D_i = 46$ lb, using a value of -1 deg for the mean change in angle of attack. From data in Roskam,[16] the drag on the craft flying alone would be 264.5 lb; we thus see an average reduction of 17.4% . This would not be fully realized in practice because of the variations in angle of attack, the control activity, and other factors.

The vertical channel results for the same case with a noisy moment measurement are shown in Fig. 13 and the lateral channel in Fig. 14. The noise is zero mean, with covariance 100. In both cases, the results are very similar to those without noise. The moment measurement and estimate are displayed in Fig. 15. As expected, the convergence is slightly delayed, but the tracking and performance are only slightly degraded.

V. Conclusions

In this paper, an improved peak-seeking scheme using modern estimation techniques is proposed. By employing a Kalman filter, the scheme rejects noise systematically and allows the estimate of the gradients as well as the sign to be used. The technique is applied to a simplified aircraft drag-reduction problem, using realistic aircraft dynamics and including the dominant nonlinear terms caused by the aircraft interaction. In simulation, the controller readily finds and maintains the optimal position for drag reduction in a two-aircraft formation.

Acknowledgments

This work was supported by the NASA Dryden Flight Research Center under Contract Number NAS4-00051. Further support was provided by the Air Force Office of Scientific Research under Grant Number F49620-96-1-0471, administered by the California Institute of Technology.

References

[1]Houghton, E. L., and Carpenter, P. W., *Aerodynamics for Engineering Students*, 4th ed., Wiley, New York, 1993, pp. 280–281.

[2]Prandtl, L., and Tietjens, O. G., *Applied Hydro- and Aeromechanics*, Dover, New York, 1957, pp. 210–222.

[3]Hummel, D., "The Use of Aircraft Wakes to Achieve Power Reductions in Formation Flight," *The Characterisation & Modification of Wakes from Lifting Vehicles in Fluids*, AGARD Conference Proceedings 584, The Advisory Group for Aerospace Research and Development, Neuilly-sur-Seine, France, 1996, pp. 36.1–36.13.

[4]Wolfe, J. D., Chichka, D. F., and Speyer, J. L., "Decentralized Controllers for Unmanned Aerial Vehicle Formation Flight," AIAA Paper 96-3833, July 1996.

[5]Chichka, D., and Speyer, J., "Solar-Powered Formation-Enhanced Aerial Vehicle Systems for Sustained Endurance," *Proceedings of the 1998 American Control Conference*, American Control Council, Dayton, OH, 1998, pp. 684–688.

[6]Pachter, M., D'Azzo, J. J., and Proud, A. W., "Tight Formation Flight Control," *Journal of Guidance, Control, and Dynamics*, Vol. 24, No. 2, 2001, pp. 246–254.

[7]LeBlanc, M., "Sur l'Electrification des Chemins de fer au Moyen de Courants Alternatifs de Frequence Elevee," *Revue Generale de l'Electricite*, France, 1922.

[8]Åström, K., and Wittenmark, B., *Adaptive Control*, Addison Wesley Longman, Reading, MA, 1989.

[9]Krstić, M., and Wang, H-H., "Design and Stability Analysis of Extremum Seeking Feedback for General Nonlinear Systems," *Proceedings of the 36th Conference on Decision and Control*, IEEE Publications, Piscataway, NJ, 1997, pp. 1743–1748.

[10]Wang, H-H., Yeung, S., and Krstić, M., "Experimental Application of Extremum Seeking on an Axial-Flow Compressor," *Proceedings of the American Control Conference*, American Control Council, Dayton, OH, 1998, pp. 1989–1993.

[11]Banaszuk, A., Zhang, Y., and Jacobson, C. A., "Adaptive Control of Combustion Instability Using Extremum Seeking," *Proceedings of the American Control Conference*, American Control Council, Dayton, OH, 2000, pp. 416–422.

[12]Walsh, G. C., "On the Application of Multi-Parameter Extremum Seeking Control," *Proceedings of the American Control Conference*, American Control Council, Dayton, OH, 2000, pp. 411–415.

[13]Rotea, M.,"Analysis of Multivariable Extremum Seeking Algorithms," *Proceedings of the American Control Conference*, American Control Council, Dayton, OH, 2000, pp. 433–437.

[14]Karamcheti, K., *Principles of Ideal-Fluid Aerodynamics*, Krieger, Malabar, FL, 1980, Chap. 19.

[15]Katz, J., and Plotkin, A., *Low-Speed Aerodynamics; from Wing Theory to Panel Methods*, McGraw–Hill, New York, 1991.

[16]Roskam, J., *Aircraft Dynamics and Control*, Roskam Aviation and Engineering Corp., Ottawa, KS, 1979, pp. 590–592.

[17]Blake, W., and Multhopp, D., "Design, Performance, and Modelling Considerations for Close Formation Flight," AIAA Paper 98-4343, July 1998.

[18]Blake, W. B., and Gingras, D. R., "Comparison of Predicted and Measured Formation Flight Interference Effects," *Journal of Aircraft*, Vol. 41, No. 2, 2004, pp. 201–207.

[19]Chichka, D. F., Speyer, J. L., and Park, C. G., "Peak-Seeking Control with Application to Formation Flight," *Proceedings of the 38th Conference on Decision and Control*, IEEE Publications, Piscataway, NJ, 1999, pp. 2463–2470.

[20]Gustafson, D., and Speyer, J., "Linear Minimum Varience Filters Applied to Carrier Tracking," *IEEE Transactions on Automatic Control*, Vol. AC-21, No. 1, Feb. 1976, pp. 65–73.

[21]Rhee, I., and Speyer, J., "Application of a Game Theoretic Controller to a Benchmark Problem," *Journal of Guidance, Control, and Dynamics*, Vol. 15, No. 5, 1992, pp. 1076–1081.